Russell, A. R. & Buzzi, O. *Géotechnique* [http://dx.doi.org/10.1680/geot.10.P.119]

TECHNICAL NOTE

A fractal basis for soil-water characteristics curves with hydraulic hysteresis

A. R. RUSSELL* and O. BUZZI†

A soil-water characteristic curve with hydraulic hysteresis is derived using fractals by treating pores as either bodies or throats. As suction is increased along the main drying curve, drying of a body is controlled by the largest throat connected to it. As suction is reduced along the main wetting curve, the absorbed water collects in the smallest bodies and throats first, and then fills larger bodies and throats in order of size. The curve is fitted to data for a silt loam. The fit is reasonable for main drying and wetting curves, but less good for scanning curves.

KEYWORDS: fractals; partial saturation; suction

On effectue la dérivation d'une courbe caractéristique sol/eau, avec hystérésis hydraulique, à l'aide de dimensions fractales, en traitant les pores comme des corps ou des gorges. Au fur et à mesure de l'augmentation de l'aspiration le long de la courbe de séchage principale, le séchage d'un corps est contrôlé par la gorge la plus grande raccordée à ce dernier. Lors de la réduction de l'aspiration le long de la courbe de mouillage principale, l'eau absorbée se recueille tout d'abord dans les corps et gorges les plus petits, avant de remplir par ordre de taille les corps et gorges plus petits. La courbe est adaptée pour des données pour un limon fin, l'adaptation étant raisonnable pour les courbes de séchage et mouillage principales, mais moins bonne pour des courbes de scannage.

INTRODUCTION

A soil-water characteristic curve (SWCC) relates suction to water content or degree of saturation, and is important in understanding water storage in the ground and soil strength variations in infrastructure (Khalili & Zargarbashi, 2010).

SWCCs depend on pore size distributions (Gitirana & Fredlund, 2004; Marinho, 2005), and many expressions have been derived by soil scientists using fractals, motivated by self-similar fractal geometry of pore sizes measured experimentally (Tyler & Wheatcraft, 1989; Perfect & Kay, 1995; Bird *et al.*, 2000; Hunt & Gee, 2002, Perfect, 2005; Wang *et al.*, 2005; Cihan *et al.*, 2007; Yu *et al.*, 2009; Russell, 2010). A fractal pore size distribution exists when the number of pores larger than a given size is proportional to that size in a power law, with the exponent representing the fractal dimension. Fractal-based SWCCs are appealing, as the defining parameters are linked to microstructural properties.

However, most SWCCs used within the geotechnical engineering community are phenomenological in origin (Wheeler *et al.*, 2003; Gitirana & Fredlund, 2004; Khalili *et al.*, 2008; Pedroso & Williams, 2010). Although they may model hysteresis (Li, 2005), or incorporate grain size descriptors (Kamiya *et al.*, 2003), they rely on fitting parameters with no direct link to microstructural properties.

Here a new fractal description of pore size distributions is presented for non-swelling soils, and is used to define separate wetting, drying and scanning curves. Deriving a SWCC using fractals is not new but, for the first time, the hysteretic loop observed during a drying–wetting–drying cycle is captured. The defining parameters are linked to microstructural properties. The SWCC is compared with experimental data.

Manuscript received 9 November 2010; revised manuscript accepted 6 July 2011.
Discussion on this paper is welcomed by the editor.
* Centre for Infrastructure Engineering and Safety, School of Civil and Environmental Engineering, The University of New South Wales, Sydney, Australia.
† Centre of Geotechnical and Materials Modelling, The University of Newcastle, Callaghan, Australia.

A FRACTAL DESCRIPTION OF A SOIL CONTAINING PORE BODIES AND PORE THROATS

In this study, pores are classified as either bodies or throats (similar to Conner *et al.*, 1986; Tsakiroglou & Ioannidis, 2008). A body has a number of smaller throats connected to it. A body cannot change to be a throat, or vice versa. Bodies and throats of different sizes exist, and obey fractal distributions. Each body or throat size is denoted by an order. Order k represents the largest size, order $k-1$ represents the second largest size and so on, down to order 0 representing the smallest size.

In a soil of volume V, throats and bodies of order k have an overall volume μV, where μ is a material parameter. μV is divided into parts belonging to throats and bodies, μqV and $\mu(1-q)V$ respectively, where q is a material parameter. μ and q are assumed constant for all orders of size.

The total numbers of bodies (or throats) of order k (with size d_k) are found by dividing the total volume of bodies (or throats) by that of a single body (or throat), which is assumed equal to Λd_k^3. Λ is a dimensionless geometric shape factor, assumed constant for all bodies and throats, and is unimportant in the derivations that follow. The total numbers of bodies or throats of order k become $\mu(1-q)V/(\Lambda d_k^3)$ and $\mu qV/(\Lambda d_k^3)$ respectively. n represents the ratio between individual body or throat volumes of successive orders (a material constant) so that bodies and throats of order $k-1$ have size $d_k/n^{1/3}$. The total volumes of bodies and throats of order $k-1$ are $\mu p(1-q)V$ and μpqV respectively, where p represents the ratio between total body (or throat) volumes of successive orders (a material constant). The total numbers of bodies and throats of order

$k-1$ are then $\mu np(1-q)V/(\Lambda d_k^3)$ and $\mu npqV/(\Lambda d_k^3)$ respectively. The same procedure can be followed for all orders to create fractal distributions, with results for the first three and ith orders presented in Table 1. μ and p are related to the porosity of the soil ϕ through

$$\phi = \frac{\mu}{1-p} \tag{1}$$

The total numbers of bodies and throats of size L larger than d_{bi} and d_{ti} (where d_{bi} and d_{ti} denote sizes of bodies and throats of order i) are

$$N_b(L > d_{bi}) = \frac{\mu(1-q)V}{\Lambda d_k^3}\left[1 + np + (np)^2 + \ldots + (np)^{k-i}\right] = \frac{\mu(1-q)V(np)^{(k-i)}}{\Lambda d_k^3}\sum_{j=0}^{k-i}\frac{1}{(np)^j} \tag{2}$$

$$N_t(L > d_{ti}) = \frac{\mu qV}{\Lambda d_k^3}\left(1 + np + (np)^2 + \ldots + (np)^{k-i}\right) = \frac{\mu qV(np)^{(k-i)}}{\Lambda d_k^3}\sum_{j=0}^{k-i}\frac{1}{(np)^j} \tag{3}$$

Subscripts b and t indicate an association with bodies and throats respectively. For $np > 1$ (a mathematical requirement of fractal geometries) these simplify to

$$N_b(L > d_{bi}) = \frac{\mu(1-q)V(np)^{(k-i)}}{\Lambda d_k^3}\left(\frac{np}{np-1}\right) \tag{4}$$

$$N_t(L > d_{ti}) = \frac{\mu qV(np)^{(k-i)}}{\Lambda d_k^3}\left(\frac{np}{np-1}\right) \tag{5}$$

From equations (4) and (5), when a large number of orders exist, the ratio of the number of bodies or throats of order $i-1$ or higher to the number of bodies or throats of order i or higher is np. Recall also that the ratio of the body or throat size of order $i-1$ to body or throat size of order i is $n^{-1/3}$. For distributions of body or throat sizes obeying the fractal distributions

$$N_b(L > d_b) \propto d_b^{-D_b} \tag{6a}$$

and

$$N_t(L > d_t) \propto d_t^{-D_t} \tag{6b}$$

where D_b and D_t denote the fractal dimensions of the bodies and throats respectively, the fractal dimensions are equal and given by

$$D_b = D_t = D = 3\left(1 + \frac{\ln p}{\ln n}\right) \tag{7}$$

The material parameters are summarised in Table 2 with their meanings and ranges of permissible values.

FROM FRACTAL PORE BODIES AND THROATS TO A SOIL-WATER CHARACTERISTIC CURVE

The SWCC comprises a main wetting curve, a main drying curve and scanning curves. Derivations are made with reference to Figs 1 and 2. Fig. 1 presents curves in the double logarithmic suction against degree of saturation ($\ln s$–$\ln S_r$) plane. Seven different stages during a wetting–drying–wetting cycle are labelled I to VII. Fig. 2 shows a simple idealised connected sequence of bodies and throats of different sizes at the seven stages, starting from an arbitrary position on the main wetting curve (Stage I). The sizes and

Table 1. Successive orders of pore bodies and throats and their geometrical properties

Order	k	$k-1$	$k-2$	...	i
Pore body/throat size	d_k	$d_k/n^{1/3}$	$d_k/n^{2/3}$	...	$d_k/n^{(k-i)/3}$
Volume of pore bodies	$\mu(1-q)V$	$\mu p(1-q)V$	$\mu p^2(1-q)V$	...	$\mu p^{(k-i)}(1-q)V$
Volume of pore throats	μqV	μpqV	$\mu p^2 qV$		$\mu p^{(k-i)}qV$
Number of bodies	$\mu(1-q)V/(\Lambda d_k^3)$	$\mu(1-q)Vnp/(\Lambda d_k^3)$	$\mu(1-q)V(np)^2/(\Lambda d_k^3)$	...	$\mu(1-q)V(np)^{(k-i)}/(\Lambda d_k^3)$
Number of throats	$\mu qV/(\Lambda d_k^3)$	$\mu qVnp/(\Lambda d_k^3)$	$\mu qV(np)^2/(\Lambda d_k^3)$	...	$\mu qV(np)^{(k-i)}/(\Lambda d_k^3)$

Table 2. Material parameters, their meaning and permissible values, as well as values that fit the data of Topp (1971)

Parameter	Meaning	Permissible values	Fit to Topp (1971) data
μ	Ratio between the volume of all pores (bodies and throats) of order k to the overall soil volume	0 to 1	0·11
q	Ratio between the volume of throats of order i and the volume of bodies plus throats of order i	0 to 1	0·14
n	Ratio between individual body or throat volumes of successive orders	$> 1/p$ and > 0	56·2
p	Ratio between total body or throat volumes of successive orders	$> 1/n$ and > 0	0·76
ϕ	Soil porosity, $\mu/(1-p)$	0 to 1	0·44
D	Fractal dimension of bodies and throats, $3(1 + \ln p/\ln n)$	2 to 3	2·80
α	Slopes of main wetting and drying curves in the $\ln s$–$\ln S_r$ plane, $-(3-D)$	0 to -1	$-0·2$
β	Slopes of scanning curves in the $\ln s$–$\ln S_r$ plane, $\frac{\ln[(1-q)+q(1/n^{1/3})^{3-D}]}{\ln(n^{1/3})}$	0 to -1	$-0·025$
s_{ex}	Air expulsion suction, $-4T\cos\theta/d_{max}$	> 0	1·7 kPa
s_{ae}	Air entry suction, $s_{ex}n^{\frac{1}{3}\left(1-\frac{\beta}{\alpha}\right)}$	> 0	5·5 kPa

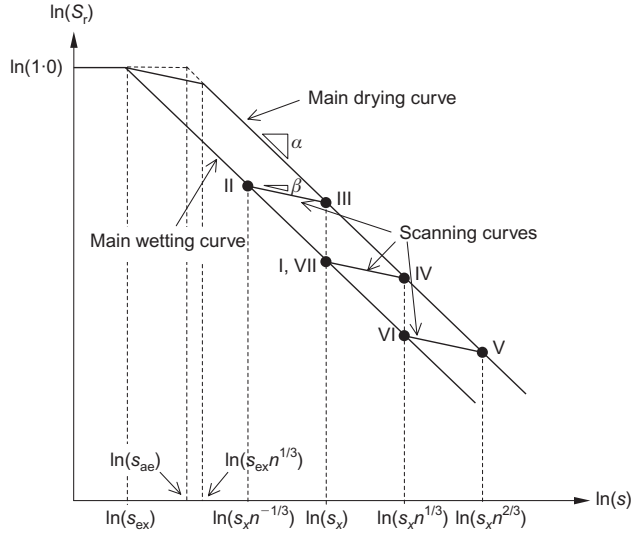

Fig. 1. The main wetting and drying curves and a number of scanning curves in the double logarithmic suction–degree of saturation ($\ln s$–$\ln S_r$) plane. Seven different stages (numbered upwards from I to VII) during a wetting–drying–wetting cycle are labelled

volumes of bodies and throats are labelled in Fig. 2. A grey body or throat indicates wet, and white indicates dry.

The assumed linear connection of smaller and larger pores in Fig. 2 is highly idealised, and not an exact representation of pore connectivity in soils, where most bodies are connected to more than two throats, permitting a multidimensional emptying/filling pattern. The idealisation is useful to study pore scale properties influencing macroscopic measurements of soil-water retention.

During wetting, absorbed water collects in the smallest bodies and throats first, and then gradually fills larger bodies and throats in order of size. This is not influenced by bodies being connected to smaller throats, as all parts of the body and throat spaces are assumed accessible (Conner *et al.*, 1986).

At Stage I, where the (s, S_r) state is on the main wetting curve and $s = s_x$, all bodies and throats larger than or equal to d_x are dry, as s_x ensures that bodies and throats of size d_x do not fill with water. Therefore all bodies and throats of size $d_x/n^{1/3}$ or smaller have filled when $s = s_x$. There is an inverse proportionality between s_x and the smallest drained pore size d_x. Notice that pores are filled even if they are not connected, as absorbed water collects in the smallest bodies and throats first, and then fills larger bodies and throats (Conner *et al.*, 1986). This seems at odds with Fig. 2. However, as already mentioned, real soils have more pore connections than that shown in this simplified representation, permitting successively larger pores to be filled in order of size.

Stage II is reached by further wetting and reducing s to $s_x/n^{1/3}$: the value associated with bodies or throats one order larger. While moving from Stage I to II, the state stays on the main wetting curve.

The volumes of wetted bodies and throats can be expressed in incremental form as

$$\delta V_b = -\Lambda C D d_b^{2-D} \delta d_b \tag{8a}$$

and

$$\delta V_t = -\Lambda C D d_t^{2-D} \delta d_t \tag{8b}$$

Before integrating these terms to find S_r (as in Russell, 2010), simplifications are introduced, noting that, during wetting, bodies and throats of a certain size can be treated as the one pore unit, and supposing that the smallest body or throat size is so small that it can be assumed to have null size. It follows that the values of S_r at Stage I, when $s = s_x$, and at Stage II, when $s = s_x/n^{1/3}$, are

$$S_{r(I)} = \left(\frac{d_x/n^{1/3}}{d_{max}}\right)^{3-D} \tag{9a}$$

and

$$S_{r(II)} = \left(\frac{d_x}{d_{max}}\right)^{3-D} \tag{9b}$$

in which d_{max} is the largest pore size. In the $\ln s$–$\ln S_r$ plane the slope of the main wetting curve is

$$\alpha = \frac{\ln\left(S_{r(II)}\right) - \ln\left(S_{r(I)}\right)}{\ln\left(s_{(II)}\right) - \ln\left(s_{(I)}\right)} = -(3 - D) \tag{10}$$

A more general definition for the main wetting curve is

$$S_r = \begin{cases} 1 & \text{for } s < s_{ex} \\ \left(\dfrac{s}{s_{ex}}\right)^{D-3} & \text{for } s > s_{ex} \end{cases} \tag{11}$$

in which s_{ex} is the suction associated with air expulsion in the largest pores,

$$s_{ex} = -\frac{4T\cos\theta}{d_{max}} \tag{12}$$

where T is the surface tension of water and θ is the contact angle between water and soil.

Stage III on the main drying curve is reached by increasing s to s_x. Because a body is connected to a number of throats, drying of a body is controlled by the largest throat connected to it. It is enough that the largest throat drains for the body to drain. Therefore the largest throat size (rather than body size) must be directly related to the s at which the body drains. At Stage III, bodies of size $d_x n^{1/3}$ have drained, as have the largest throats of size d_x connected to them. S_r is then

$$S_{r(III)} = (1 - q)\left(\frac{d_x}{d_{max}}\right)^{3-D} + q\left(\frac{d_x/n^{1/3}}{d_{max}}\right)^{3-D} \tag{13}$$

Stage IV is reached following further drying, to when $s = s_x n^{1/3}$. Stage V is reached following even more drying, to when $s = s_x n^{2/3}$. While moving from Stage III to Stage V, the state stays on the main drying curve. The values of S_r at Stages IV and V are

$$S_{r(IV)} = (1 - q)\left(\frac{d_x/n^{1/3}}{d_{max}}\right)^{3-D} + q\left(\frac{d_x/n^{2/3}}{d_{max}}\right)^{3-D} \tag{14a}$$

and

$$S_{r(V)} = (1 - q)\left(\frac{d_x/n^{2/3}}{d_{max}}\right)^{3-D} + q\left(\frac{d_x/n}{d_{max}}\right)^{3-D} \tag{14b}$$

The slope of the main drying curve is also $-(3 - D)$, and a general definition is

$$S_r = \begin{cases} 1 & \text{for } s < s_{ae} \\ \left(\dfrac{s}{s_{ae}}\right)^{D-3} & \text{for } s > s_{ae} \end{cases} \tag{15}$$

in which s_{ae} is suction associated with air entry. To establish

Fig. 2. A connected sequence of pore bodies and throats of different sizes at the seven different stages of wetting and drying, starting from Stage I (an arbitrary position on the wetting curve). The sizes and volumes of the pore bodies and throats are labelled but not drawn to scale. A grey pore body or throat indicates it is wet, and white indicates dry

the relationship between s_{ae} and s_{ex}, notice that $n^{1/3}$ represents the ratio between s on the main wetting curve when $S_r = 1$ and s on the main drying curve after the largest pore throats have drained (Fig. 1). It follows that

$$s_{ae} = s_{ex} n^{\frac{1}{3}\left(1-\frac{\beta}{\alpha}\right)} \tag{16}$$

Equations (11) and (15) happen to be of the same form as the Brooks & Corey (1964) SWCC when the residual S_r is zero.

Moving from Stage II to Stage III, or more generally as wetting is changed to drying and the state moves from the main wetting curve to the main drying curve (or vice versa), the state moves along a scanning curve. When straight in the $\ln s$–$\ln S_r$ plane, all scanning curves have the slope

$$\beta = \frac{\ln\left(S_{r(III)}\right) - \ln\left(S_{r(II)}\right)}{\ln\left(s_{(III)}\right) - \ln\left(s_{(II)}\right)} = \frac{\ln\left[(1-q) + q\left(\frac{1}{n^{1/3}}\right)^{3-D}\right]}{\ln\left(n^{1/3}\right)} \tag{17}$$

The state when $S_r = 1$ and $s = s_{ae}$ is inaccessible, as the largest throats drain as soon as s is increased above s_{ex}. The inaccessible region is bound by the dashed line in Fig. 1. s_{ae} is dependent on d_{max} as well as on the other material parameters n, q and D.

In studies by Perfect (2005) and Cihan *et al.* (2007), different assumptions regarding geometry and interconnectivity of pores and drainage sequences were made. Although they attributed hysteresis to incomplete drying of pores of a certain size as suction increases, as is also done here, their derivation and validation were limited to the main drying curve. Their expression for scale-invariant draining becomes the same as equation (15) when their parameter P, control-

ling the volumetric fraction of pores of a certain size that drain at a certain suction, is equal to q and ϕ, noting that s_{ae} and their h_{min} have the same role. However, influences of $n^{1/3}$ and their scale parameter b on the relative magnitudes of s_{ae} and s_{ex} may differ slightly, as the slight lowering of S_r due to drainage of the largest throats prior to the largest bodies is allowed in this study, but not in theirs.

The SWCC is now fitted to data for a silt loam from Topp (1971) in Fig. 3. The main drying and wetting curves have been fitted, by trial and error, using the material parameters listed in Table 2. The constant slope for scanning curves does not permit a good fit. However, constant slopes are appealing and convenient, especially for computational analyses involving coupled hydro-mechanical behaviour. The intention is not to achieve perfection, but to present an adequate and simple explanation of soil-water characteristics based on fractals.

CONCLUSION

The pore space may be modelled by treating pores as either bodies or throats. Fractal distributions for bodies and throats may be defined, and fractal dimensions become equal when the ratio of body and throat numbers at all size scales is constant.

The fractal definitions permit derivation of main wetting and drying curves. As s is increased along the main drying curve, drying of a body is controlled by the largest of the

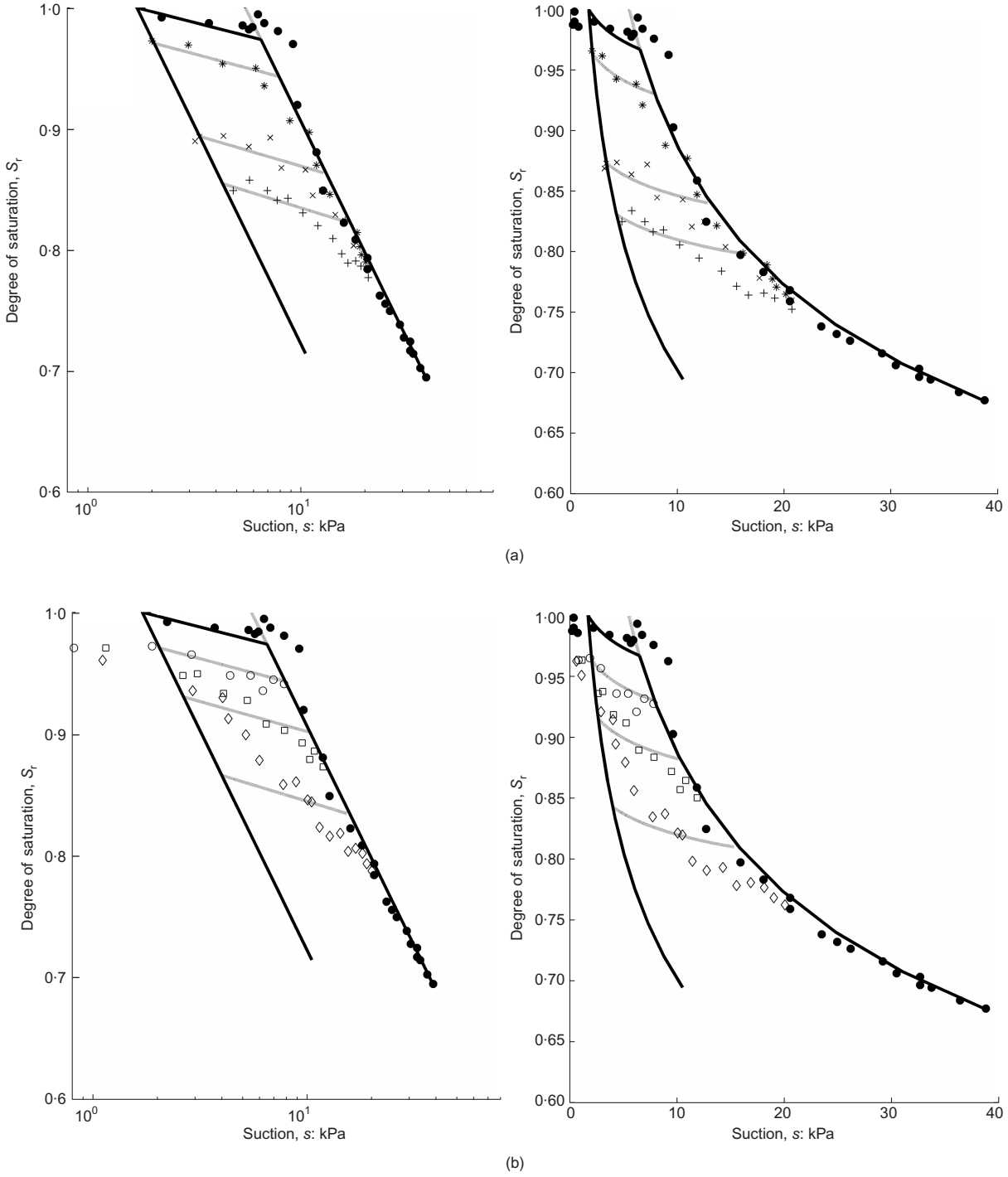

Fig. 3. The SWCC fitted to the data of Topp (1971) for a silt loam: (a) scanning data are for drying paths, (b) scanning data are for wetting paths

throats connected to it. As s is reduced along the main wetting curve, water collects in the smallest bodies and throats first, and then fills larger bodies and throats. The curves are straight lines in the $\ln s - \ln S_r$ plane, and have slopes that are functions of the fractal dimension. Scanning curves arise, and have slopes dependent on the volumetric fraction of throats and fractal properties.

For real soils there would be natural rounding of the sharp corners, and repeated drying–wetting reversals may show a slight non-linearity. In any case, the analysis shows how the general features of the SWCC may be linked to fractal pore scale characteristics.

NOTATION

C	constant of proportionality
D_b, D_t	fractal dimensions of bodies and throats respectively
d_{bi}, d_{ti}	sizes of bodies and throats of order i
d_k	size of bodies of order k
d_{max}	largest pore size
d_x	the largest drained pore size when suction is s_x
k	order of largest size
L	size of body or throat
N_b, N_t	total numbers of bodies and throats
n	ratio between individual body or throat volumes of successive orders
p	ratio between total body (or throat) volumes of successive orders
q	material parameter
S_r	degree of saturation
s	suction
s_{ae}	suction associated with air entry
s_{ex}	suction associated with air expulsion
s_x	an arbitrary suction
T	surface tension of water
V	overall soil volume
V_b, V_t	volumes of wetted bodies and throats
α	slope of main wetting curve
θ	contact angle between water and soil
Λ	dimensionless geometric shape factor
μ	material parameter
ϕ	porosity of soil

REFERENCES

Bird, N. R. A., Perrier, E. & Rieu, M. (2000). The water retention function for a model of soil structure with pore and solid fractal distributions. *Eur. J. Soil Sci*. **51**, No. 1, 55–63.

Brooks, R. H. & Corey, A. T. (1964). *Hydraulic properties of porous media*, Hydrology Paper 3, pp. 22–27. Fort Collins, CO: Colorado State University.

Cihan, A., Perfect, E. & Tyner, J. S. (2007). Water retention models for scale-variant and scale invariant drainage of mass prefractal porous media. *Vadose Zone J.* **6**, No. 4, 786–792.

Conner, W. C., Cevallos-Candau, J. F., Weist, E. L., Pajares, J., Mendioroz, S. & Cortés, A. (1986). Characterization of pore structure: porosimetry and sorption. *Langmuir* **2**, No. 2, 151–154.

Gitirana, G. Jr & Fredlund, D. G. (2004). Soil-water characteristic curve equation with independent properties. *J. Geotech. Geoenviron. Engng* **130**, No. 2, 209–212.

Hunt, A. G. & Gee, G. W. (2002). Application of critical path analysis to fractal porous media: comparison with examples from the Hanford site. *Adv. Water Resour.* **25**, No. 2, 129–146.

Kamiya, K., Uno, T. & Saso, T. (2003). Influence from grain size distribution to moisture characteristic curve. *Proc. 2nd Asian Conf. on Unsaturated Soils, Osaka*, 441–444.

Khalili, N. & Zargarbashi, S. (2010). Influence of hydraulic hysteresis on effective stress in unsaturated soils. *Géotechnique* **60**, No. 9, 729–734, http://dx.doi.org/10.1680/geot.9.T.009.

Khalili, N., Habte, M. A. & Zargarbashi, S. (2008). A fully coupled flow deformation model for cyclic analysis of unsaturated soils including hydraulic and mechanical hysteresis. *Comput. Geotech*. **35**, No. 6, 872–889.

Li, X. S. (2005). Modelling of hysteresis response for arbitrary wetting/drying paths. *Comput. Geotech*. **32**, No. 2, 133–137.

Marinho, F. A. M. (2005). Nature of soil–water characteristic curve for plastic soils. *J. Geotech. Geoenviron. Engng* **131**, No. 5, 654–661.

Pedroso, D. M. & Williams, D. J. (2010). A novel approach for modelling soil-water characteristic curves with hysteresis. *Comput. Geotech*. **37**, No. 3, 374–380.

Perfect, E. (2005). Modelling the primary drainage curve of prefractal porous media. *Vadose Zone J.* **4**, No. 4, 959–966.

Perfect, E. & Kay, B. D. (1995). Applications of fractals in soil and tillage research: a review. *Soil and Tillage Res*. **36**, Nos 1–2, 1–20.

Russell, A. R. (2010). Water retention characteristics of soils with double porosity. *Eur. J. Soil Sci*. **61**, No. 3, 412–424.

Topp, G. C. (1971). Soil water hysteresis in silt loam and clay loam soils. *Water Resour. Res*. **7**, No. 4, 914–920.

Tsakiroglou, C. D. & Ioannidis, M. A. (2008). Dual-porosity modelling of the pore structure and transport properties of contaminated soil. *Eur. J. Soil Sci*. **59**, No. 4, 744–761.

Tyler, S. W. & Wheatcraft, S. W. (1989). Application of fractal mathematics to soil water retention estimation. *Soil Sci. Soc. Am. J.* **53**, No. 4, 987–996.

Wang, K., Zhang, R. & Wang, F. (2005). Testing the pore-solid fractal model for the soil water retention function. *Soil Sci. Soc. Am. J.* **69**, No. 3, 776–782.

Wheeler, S. J., Sharma, R. S. & Buisson, M. S. R. (2003). Coupling of hydraulic hysteresis and stress–strain behaviour in unsaturated soils. *Géotechnique* **53**, No. 1, 41–54, http://dx.doi.org/10.1680/geot.2003.53.1.41.

Yu, B., Cai, J. & Zou, M. (2009). On the physical properties of apparent two-phase fractal porous media. *Vadose Zone J.* **8**, No. 1, 177–186.